The Polyelectrolyte Behavior of Actin Filaments: A ^{25}Mg NMR Study†

Wujing Xian,*,‡,§ Jay X. Tang,|| Paul A. Janmey,|| and William H. Braunlin‡,⊥

Department of Chemistry, The University of Nebraska-Lincoln, Lincoln, Nebraska 68588-0304, and Hematology Division, Brigham and Women's Hospital, 221 Longwood Avenue, Boston, Massachusetts 02115

Received September 24, 1998; Revised Manuscript Received March 26, 1999

ABSTRACT: Under physiological conditions, filamentous actin (F-actin) is a polyanionic protein filament. Key features of the behavior of F-actin are shared with other well-characterized polyelectrolytes, in particular, duplex DNA. For example, the bundle formation of F-actin by polyvalent cations, including divalent metal ions such as Mg^{2+}, has been proposed to be a natural consequence of the polyelectrolyte nature of actin filaments [Tang and Janmey (1996) *J. Biol. Chem. 271*, 8556−8563]. This recently proposed model also suggests that weak interactions between F-actin and Mg^{2+} ions reflect a nonspecific trapping of counterions in the electric field surrounding F-actin due to its polyelectrolyte nature. To test this hypothesis, we have performed ^{25}Mg NMR measurements in F-actin solutions. Based on the NMR data, we estimate that the rotational correlation times of Mg^{2+} are independent of the overall rotational dynamics of the actin filaments. Moreover, competitive binding experiments demonstrate a facile displacement of F-actin-bound Mg^{2+} by $Co(NH_3)_6^{3+}$. At higher $Co(NH_3)_6^{3+}$ concentrations, a fraction of the magnesium ions are trapped as actin filaments aggregate. ATP also competes effectively with actin filaments for binding to Mg^{2+}. These results support the hypothesis that magnesium ions bind loosely and nonspecifically to actin filaments, and thus show a behavior typical of counterions in polyelectrolyte solutions. The observed features mimic to some extent the well-documented behavior of counterions in DNA solutions.

Many biological macromolecules are polyelectrolytes, for example, DNA, RNA, charged polysaccharides, filamentous protein assemblies such as F-actin and microtubules, and viruses such as the bacteriophage fd and the tobacco mosaic virus (TMV). In solution, counterions accumulate in the vicinity of polyelectrolytes to balance the local charge. Several useful polyelectrolyte theories have been developed based on the cylindrical-rod cell model, which in its primitive form postulates that electrical charges are distributed uniformly along the length of the polyelectrolyte *(1)*. A specific polyelectrolyte is characterized by a dimensionless linear charge density, ξ, defined as the ratio between the Bjerrum length λ_B and the linear charge spacing b on the polyelectrolyte. In the classical theory of simple electrolyte solutions, the Bjerrum length is a characteristic interaction distance for ion-pair formation *(2)*, defined by

$$\lambda_B = \frac{e^2}{4\pi\epsilon_0\epsilon kT}$$

where e is the elementary charge, kT is the thermal energy, ϵ_0 is the permittivity of vacuum, and ϵ is the relative dielectric constant. λ_B is 7.1 Å in water at 20 °C with a dielectric constant $\epsilon = 80$.

The counterion condensation (CC) theory of Manning provides a very useful quantitative description of the key features of polyelectrolyte-counterion interactions *(3−6)*. The thermodynamic predictions of the Manning theory and the Poisson-Boltzmann theory *(7, 8)* are identical in the limit of infinite dilution. These two theories and other approaches *(1, 9, 10)* differ in the details of counterion distribution, but are in qualitative agreement on the existence of steep counterion gradients surrounding the polyelectrolyte. Since the key features of our argument are independent of such details, we will discuss our results in terms of the conceptually attractive framework provided by CC theory.

According to CC theory, there exists a critical charge density $\xi_{crit} = 1$, above which counterions condense in a thin layer surrounding the cylinder to maintain this critical value. Such a population represents a well-defined fraction $(1 - 1/Z\xi)$ of the total polyelectrolyte charge, where Z is the valence of the counterion. For example, for duplex DNA, $b = 1.7$ Å; thus, $\xi = 4.2$, and the total phosphate charge is neutralized to an estimated 77% by the monovalent cations, or 88% if sufficient divalent cations are present in solution.

Filamentous (F)-actin is comprised of actin monomers of molecular mass 42 000 daltons, bound by specific noncovalent self-assembling sites to form a double-helical filament. Each subunit of an actin filament contains one high-affinity (K_d in the nanomolar range) divalent cation binding site that is usually occupied by Mg^{2+} in vivo. Saturation of this binding site is insufficient to promote actin polymerization, which is driven either by millimolar concentrations of Mg^{2+} or else by the order of 100 mM concentrations of monovalent ions. Assuming the amino acid sequence of α-skeletal muscle actin, each monomer subunit retains roughly 11 excess

† This work was supported by NIH grants to P.A.J. (AR38910) and W.H.B. (GM40438), and by an NIH training grant to J.X.T. (HL19429).

* Corresponding author.

‡ The University of Nebraska-Lincoln.

§ Current address: Hematology Division, Brigham and Women's Hospital, LMRC 301, 221 Longwood Ave., Boston, MA 02115.

|| Brigham and Women's Hospital.

⊥ Current address: GelTex Pharmaceuticals, Nine-Fourth Ave., Waltham, MA 02154.

10.1021/bi982301f CCC: $18.00
Published on Web 05/12/1999

negative charges in the polymerized form, and it is estimated that $b = 2.5$ Å averaged along the filament *(11)*. This value is less than the upper limit of 7.1 Å but larger than the charge spacing of 1.7 Å for DNA, suggesting that although F-actin is not as highly charged as DNA, the phenomenon of counterion condensation is still relevant. Evidence for polyelectrolyte behavior is found in the formation of paracrystalline bundles of F-actin by divalent and polyvalent cations, and it has been demonstrated *(11, 12)* that general features are analogous to the condensation of DNA *(13)*. The most convincing demonstration of counterion condensation in DNA solutions derives from studies of cation NMR relaxation dynamics *(14)*. It is therefore natural to attempt a more direct demonstration of counterion condensation on the surface of actin filaments via cation NMR studies.

The cation of focus in this report is Mg^{2+}. Monomeric actin polymerizes to form F-actin in 2 mM $MgCl_2$. At higher Mg^{2+} concentrations (>10 mM), the bundling of actin filaments occurs. Interactions between F-actin and Mg^{2+} or other divalent metal ions show characteristic polyelectrolyte features. For instance, it has been shown that approximately four or five Mg^{2+}, Ca^{2+}, or Mn^{2+} ions per actin subunit bind interchangeably to F-actin with comparably low affinities in the millimolar range *(15)*. In the original report, the data were interpreted in terms of five relatively weak but specific binding sites on each actin monomer. An alternative model is that the divalent metal ions are simply trapped as counterions in the immediate vicinity of actin filaments. According to this model, the metal ions are sequestered near the surface of the filaments, but not necessarily attached to any particular sites. Instead, the cations are free to diffuse along the filaments. This alternative hypothesis based on polyelectrolyte behavior can be tested by ^{25}Mg NMR experiments.

^{25}Mg has a spin $^5/_2$ nucleus with a nuclear electric quadrupolar moment. The interaction of the quadrupole moment with electric field gradients provides a very effective relaxation mechanism *(14, 16, 17)*. The observed line shapes are sensitive to the motional and exchange dynamics of the Mg^{2+} ions, and thus provide insights into the interaction between Mg^{2+} and the actin filaments.

MATERIALS AND METHODS

Sample Preparations. Monomeric actin was purified according to the method of Spudich and Watt *(18)*. Phalloidin was purchased from Sigma Chemical Co. (St. Louis, MO). A stock solution of 1.25 mM phalloidin in ethanol was prepared before adding to actin solutions. ^{25}Mg isotope enriched MgO was purchased from Oak Ridge National Laboratory (Oak Ridge, TN). ^{25}MgO was dissolved in HCl to prepare a $^{25}MgCl_2$ stock solution. The nonpolymerizing solution contained 2 mM HEPES buffered at pH 7.5, 0.5 mM NaN_3, 0.1 mM $CaCl_2$, and 0.1 mM ATP; a similar solution without ATP was also used as specified. To prepare actin filament solutions, aliquots of the rapidly frozen G-actin solution were first thawed and spun at 10K rpm for 5 min to remove insoluble materials; then a concentrated $MgCl_2$ stock solution was added to reach a final concentration of 2 mM in order to polymerize actin. For solutions with high actin concentrations (12 mg/mL), small amounts of gelsolin were added at a molar ratio of gelsolin:actin = 1:300 to control the length of the polymers, thereby lowering the viscosity and preventing spontaneous phase transition to a nematic liquid-crystalline phase *(19)*. The actin solutions were allowed to polymerize for 2 h at room temperature prior to NMR experiments. To allow removal of ATP without depolymerizing actin, 25 μM phalloidin was added to the actin solutions after polymerization. The solution was then dialyzed against non-ATP buffer for a few hours. About 2 mL of F-actin solution was used for each NMR experiment.

NMR Experiments. All ^{25}Mg NMR experiments were performed at 30.61 MHz on a 11.75 T GN-500 spectrometer using a 10 mm low band probe with temperature control. The temperature of all experiments was 25 °C unless specified otherwise. The dead time between the last pulse and the first data point was set to 100 μs to avoid acoustic ringing. Longitudinal relaxation times were measured by inversion recovery methods.

The quadrupolar relaxation of ^{25}Mg under the nonextreme narrowing condition is tri-exponential, giving rise to a tri-Lorentzian line shape. The line shape can be analyzed numerically using the Redfield relaxation matrix (see Appendix) *(20)*. For comparison with experimental results, we have performed such analysis using estimated rotational correlation times (τ_c) and effective quadrupole constants (χ_{eff}). Under the conditions of our experiments, χ_{eff} is closely approximated by $\chi_{eff} = \sqrt{p_b}\chi_b$ *(14)*, where p_b is the fraction of magnesium ions bound to actin and χ_b is the quadrupole constant for these bound ions. Simulations of ^{25}Mg spectra were performed by implementing the methods of Westlund and Wennerström in *Mathematica (21)*. In the simulation, the dynamic shift was introduced, which gives rise to a chemical shift difference between Figure 1B and Figure 1C. A dynamic shift is evident from the asymmetry of Figure 1C, but the precise value of the shift was difficult to determine due to its coupling with phase adjustment. Therefore, these spectra are plotted according to the dynamic shift calculated by spectra simulation.

The NMR integrated intensities were obtained by fitting the spectra to multiple Lorentzian line shapes using the spectrum analysis program *SPAN* in *Omega.* Spectra are fitted to single or double Lorentzian to give measurements of the spectra and to illustrate the narrow and broad components of the spectra. It is noted that these fitting parameters, however, are not well-defined physical parameters.

RESULTS

Binding of Mg^{2+} to ATP and Gelsolin. Effects of ATP and gelsolin on $^{25}Mg^{2+}$ were examined as control experiments. Typically, 0.1−0.5 mM ATP or ADP is maintained in actin solutions in order to prevent actin denaturation. Gelsolin is also added to control the lengths of the actin filaments by randomly severing the actin filaments and keeping the rapidly exchanging barbed end of F-actin capped. The addition of gelsolin therefore helps to reduce the solution viscosity and prevent liquid-crystalline formation of F-actin, i.e., spontaneous alignment of actin filaments, in the course of polymerization, which occurs at slightly above 2 mg/mL for well-purified actin.

Control experiments showed that gelsolin at the low concentrations introduced into the F-actin solutions does not

have a significant effect on the NMR relaxation behavior of Mg^{2+} (data not shown). ATP, on the other hand, chelates Mg^{2+} quite strongly. Therefore, studies of the binding of Mg^{2+} to actin filaments must take into account the binding of Mg^{2+} to ATP. Previous studies on Mg^{2+}-ATP interactions include the pioneering work of Bryant *(16)* using low-field NMR and natural-abundance ^{25}Mg, and more recently, work by Bock et al. *(22)* using modern high-field NMR and isotope-enriched samples. These studies have shown that the presence of ATP has a significant line-broadening effect on the $^{25}Mg^{2+}$ spectra. We repeated some of these experiments under the conditions used in our $^{25}Mg-$F-actin experiments. The results show that the ^{25}Mg NMR spectra in ATP-containing buffer solution at 10 and 30 °C are both Lorentzian, and that the line width decreases from 39.5 Hz at 10 °C to 36.2 Hz at 30 °C. This result indicates that the bound and free Mg^{2+} ions are in rapid exchange. The ^{25}Mg longitudinal relaxation time T_1 measured at 25 °C is 9.1 ms. If T_1 equals T_2, the ^{25}Mg transverse relaxation time, then this would give a natural line width ($1/\pi T_2$) of 35 Hz. This is sufficiently close to the measured inhomogeneity broadened line width of 39 Hz to confirm that the motion of ATP-bound Mg^{2+} is in the extreme narrowing region. The line broadening of the $^{25}Mg^{2+}$ spectra by ATP complicates the interpretation of the Mg^{2+}-F-actin interaction and is undesirable. In our initial studies presented here, this problem has been accommodated qualitatively. The feasibility of performing ^{25}Mg NMR experiments in ATP-free, phalloidin-stabilized F-actin solution is also explored.

Binding of Mg^{2+} to Actin Filaments. Figure 1 shows the ^{25}Mg NMR spectra of 2 mM Mg^{2+} in the presence of (A) 0.1 mM ATP and no F-actin, (B) 0.1 mM ATP and 2 mg/mL F-actin, and (C) 0.1 mM ATP and 11 mg/mL F-actin. The spectra of Mg^{2+} in both actin solutions are clearly multi-Lorentzian. The peak in the spectrum of Figure 1C is slightly shifted upfield from those in Figure 1A and Figure 1B due to a dynamic shift as mentioned previously *(20)*. Line shape analysis of these spectra gave correlation times of 21 and 42 ns for the 2 and 11 mg/mL solutions, respectively. The quantity $\chi_{eff} = \sqrt{p_b}\chi_b$ is equal to 0.3 MHz for the 2 mg/mL solution and 0.96 MHz for the 11 mg/mL solution. If we assume, as predicted by polyelectrolyte theory, that the fractional neutralization of actin negative charge by Mg^{2+} is essentially invariant, this implies a decrease in χ_b by a factor of about 1.4 upon going from a low actin concentration of 2 mg/mL to a high actin concentration of 11 mg/mL. Specifically, if as counterion condensation theory predicts, the fractional charge neutralization $r_b = 0.82$ (*11*), then for a molecular mass of 42 000 daltons and 11 negative charges per actin monomer, $p_b = 0.11$ and 0.59 for the 2 mg/mL (0.048 mM) and 11 mg/mL (0.26 mM) samples, respectively. Hence, the estimated quadrupole constants would be 0.92 and 1.25 MHz, respectively. Given the approximations of our analysis (constant p_b, isotropic rotational modulation of the quadrupolar interaction), the difference between these two numbers is small. Moreover, these values are well within the range anticipated for nonspecific association. χ_b was estimated to be 3.1 MHz by Berggren et al. (*23*) and 0.9 MHz by Wright and Lerner (*36*) in their studies on DNA-Mg^{2+} interactions. Such modest quadrupole constants would not be expected if $^{25}Mg^{2+}$ were to lose waters of hydration upon binding to F-actin.

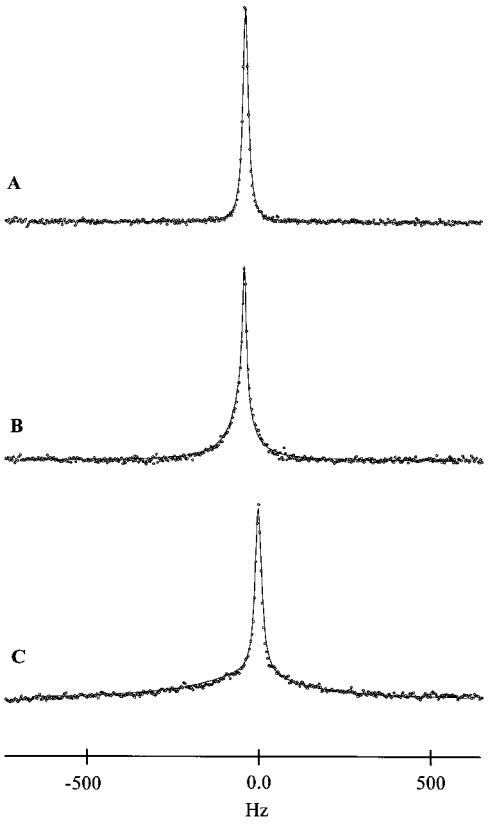

FIGURE 1: ^{25}Mg NMR spectra of 2 mM Mg^{2+} in a control buffer solution containing 0.1 mM ATP (A), polymerized 2 mg/mL actin solution (B), and polymerized 11 mg/mL actin solution (C). All three measurements were performed at 30 °C. The solid line in spectrum A is a single Lorentzian line shape. The solid lines in spectra B and C are simulations for an $I = {}^5/_2$ nucleus, performed as described in the text. The parameters of these simulations are (B) $\chi_{eff} = 0.3$ MHz, $\tau_c = 21$ ns, and (C) $\chi_{eff} = 0.96$ MHz, $\tau_c = 42$ ns. The chemical shift difference between spectra B and C is due to the dynamic shift from the simulation (see Materials and Methods).

The rotational correlation times for free Mg^{2+} ions are in the picosecond range, and those for the actin filaments are estimated to be in the millisecond range or above (*24*−*26*). Based on the simulation results above, the rotational motions of Mg^{2+} are significantly retarded in the presence of actin filaments, yet remain much more rapid than those of the filaments themselves. This result is likewise similar to that found previously for Mg^{2+} binding nonspecifically to duplex DNA.

Displacement of Mg^{2+} and Bundling of Actin Filaments by Cobalt Hexaammine. If the interaction between Mg^{2+} and actin filaments is primarily electrostatic, rather than direct and cation-specific coordination to protein carboxyl groups, for example, it should be possible to displace the Mg^{2+} ions by other multivalent cations, such as $Co(NH_3)_6^{3+}$. Figure 2 shows ^{25}Mg NMR spectra of 2 mM Mg^{2+} in an 11 mg/mL (0.26 mM) actin solution upon titration with $Co(NH_3)_6^{3+}$. The broad components of the spectra gradually decrease as more cobalt hexaammine cations are added. During the titration, the actin filaments start to form bundles at concentrations of greater than 1 mM $Co(NH_3)_6^{3+}$ (Figure 2C). The bundling is quite extensive at 1.5 mM $Co(NH_3)_6^{3+}$ (Figure 2D), and the solution becomes turbid. Table 1 shows the line widths and integrated intensities from single or double Lorentzian fit of the spectra. The difference in the

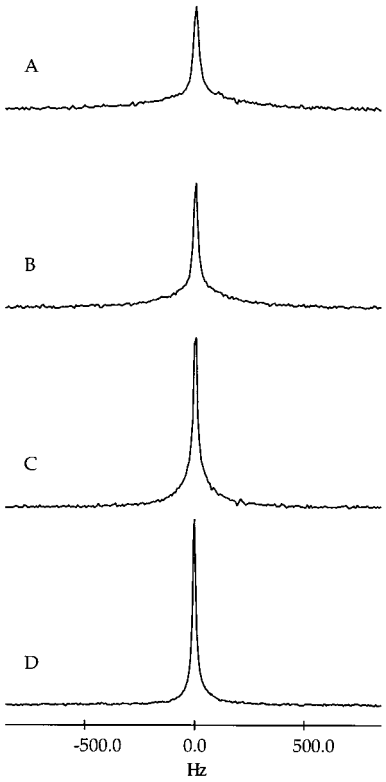

FIGURE 2: ^{25}Mg NMR spectra of 2 mM Mg^{2+} in polymerized 11 mg/mL actin solution titrated by cobalt hexaammine(III). The concentration of $Co(NH_3)_6^{3+}$ is 0.2 mM (A), 0.5 mM (B), 1.0 mM (C), and 1.5 mM (D), respectively.

Table 1: Parameters Obtained by Fitting the ^{25}Mg NMR Spectra in Figure 2 to Single or Double Lorentzian Line Shapes[a]

spectrum	I_A[b]	I_B[b]	I_{Total}[b]	W_A[b]	W_B[b]
Figure 2A	2.75	6.95	9.70	29.1	426.1
Figure 2B	2.65	6.60	9.25	23.0	311.4
Figure 2C	2.73	5.96	8.69	16.6	144.9
Figure 2D	4.08	—[b]	4.08	22.7	—

[a] For spectra that are fitted to a double Lorentzian line shape, the fitting parameters illustrate the broad component and the narrow component. [b] I_A, I_B, and I_{Total} are the integrated intensities (in arbitrary units) of the two fitted Lorentzian lines A and B, and the total intensity, respectively. W_A and W_B are the line widths of A and B in hertz, respectively. "—" indicates that the spectrum was fitted with only one Lorentzian function.

composition of the spectra in terms of narrow and broad components is clear. By fitting the presumably tri-Lorentzian line shapes of ^{25}Mg NMR spectra with bi-Lorentzian ones, the line width of each component does not have well-defined physical meaning because it does not correspond to a specific relaxation rate (*36*), but the effect of line broadening is reflected in Table 1: I_B is weighted by the broad component-(s) from the tri-Lorentzian line shape, and it decreases as a result of intensity loss of the broad component(s); meanwhile I_A does not change much until actin bundling occurs, where the broad component(s) is (are) undetectable and the line shape appears to be single Lorentzian. Figure 3 shows the normalized relative integrated intensities from Table 1 versus the cobalt hexaammine cation concentration. A noticeable change is that the integrated intensities of the $^{25}Mg^{2+}$ signals decrease markedly as the amount of $Co(NH_3)_6^{3+}$ increases. The total ^{25}Mg intensity drops more drastically at the point where the actin filaments start forming bundles, as is

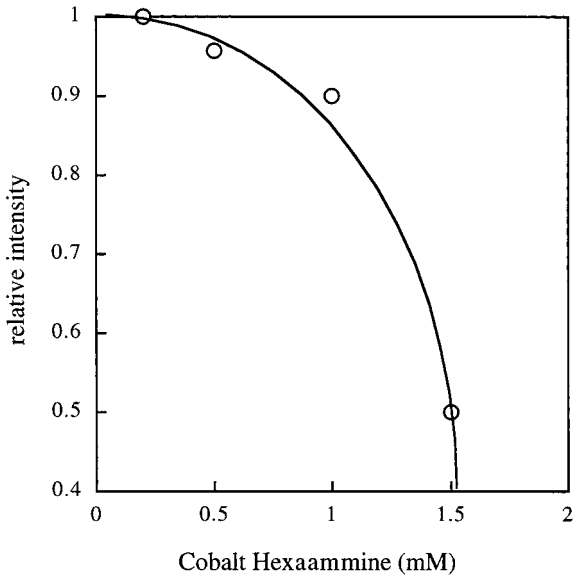

FIGURE 3: Relative integrated intensity of 2 mM Mg^{2+} in polymerized 11 mg/mL actin solution upon titration with cobalt hexaammine(III) cations. The data points are from the ^{25}Mg NMR spectra displayed in Figure 2. The sharp decrease of intensity at above 1 mM $Co(NH_3)_6^{3+}$ corresponds well to the apparent aggregation of F-actin.

anticipated if some of the Mg^{2+} ions are trapped inside the actin filament bundles and consequently become undetectable by NMR in solution.

Another feature of actin bundling, characteristic of polyelectrolyte behavior, is that it can be reversed by addition of excess monovalent cations. When 100 mM KCl is added to the solution of F-actin bundled by 1.5 mM $Co(NH_3)_6^{3+}$ and 2 mM Mg^{2+}, the solution becomes clear as the actin filament bundles dissolve. Figure 4 shows the unbundling process monitored by ^{25}Mg NMR. Two changes are observed during the dissolution of the actin filament bundles: first, the ^{25}Mg line width increases substantially; and second, the integrated intensity of the ^{25}Mg signal increases by about 20%. Both changes are expected if some of the Mg^{2+} ions are originally trapped in the bundles, but are released following the dissolution of the actin filament bundles.

Titration with ATP. ATP is a multivalent anion that binds to Mg^{2+}. For weak electrostatic binding of Mg^{2+} to actin filaments, ATP in excess is expected to compete with actin filaments for binding to Mg^{2+} ions. Figure 5 shows ^{25}Mg NMR spectra of 2 mM Mg^{2+} in 11 mg/mL actin solution titrated with ATP. As the amount of ATP increases, the line widths of both the narrow and broad components broaden significantly. Eventually the line width narrows again and the line shape becomes single Lorentzian. This concentration dependence may indicate a transition from slow to rapid exchange as the concentration of ATP is increased. As mentioned previously, ATP-bound Mg^{2+} ions exchange rapidly with free Mg^{2+} ions in the solution. The titration results confirm that ATP is able to compete effectively with the actin filaments for binding to Mg^{2+}.

Simplifying the Exchange Dynamics: Use of Phalloidin To Allow Removal of Free ATP. The presence of ATP in the buffer solution complicates the relaxation dynamics of Mg^{2+}, as demonstrated above. An F-actin solution that is free of unbound nucleotide can be obtained by first stabilizing the filaments with stoichiometric amounts of phalloidin and

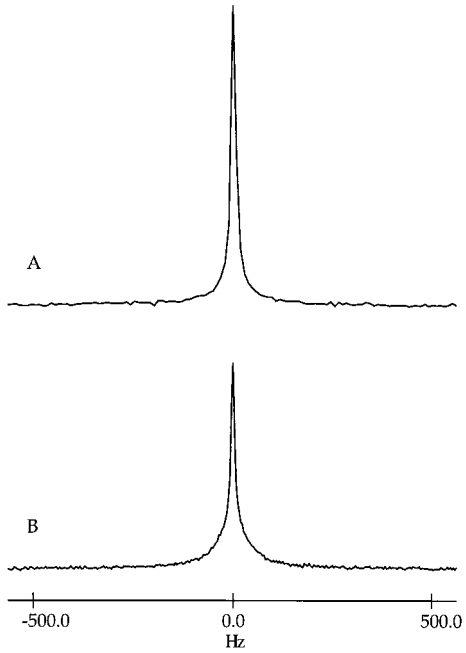

FIGURE 4: Effect of excess monovalent cations on $Co(NH_3)_6^{3+}$-induced F-actin bundling. (A) ^{25}Mg NMR spectrum of 2 mM Mg^{2+} in polymerized 11 mg/mL actin solution in which F-actin bundling was induced with 1.5 mM $Co(NH_3)_6^{3+}$ (same as Figure 2D but plotted on a different frequency scale). (B) After about 100 mM K^+ was added to the above solution which partially dissolved the F-actin bundles.

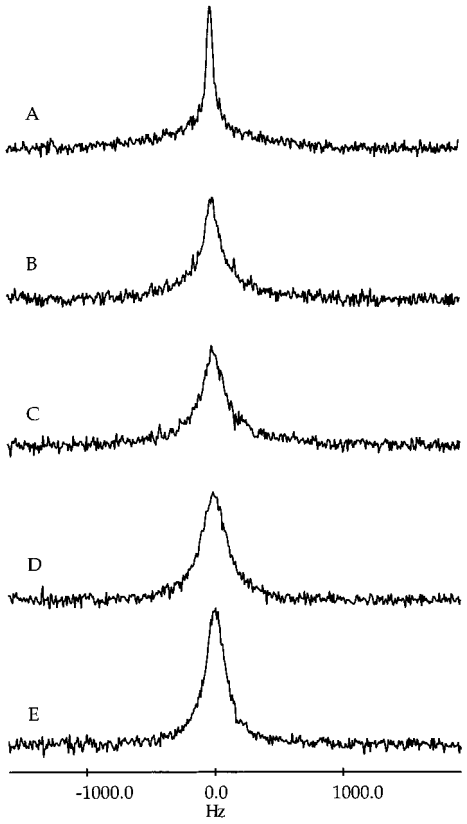

FIGURE 5: ^{25}Mg NMR spectra of 2 mM Mg^{2+} in polymerized 11 mg/mL actin solution titrated by ATP. The total concentration of ATP which includes the 0.1 mM ATP in the buffer solution is 0.1 mM (A), 0.2 mM (B), 0.3 mM (C), 0.4 mM (D), and 0.6 mM (E), respectively. (The solution condition of spectrum A was the same as that of Figure 1C.)

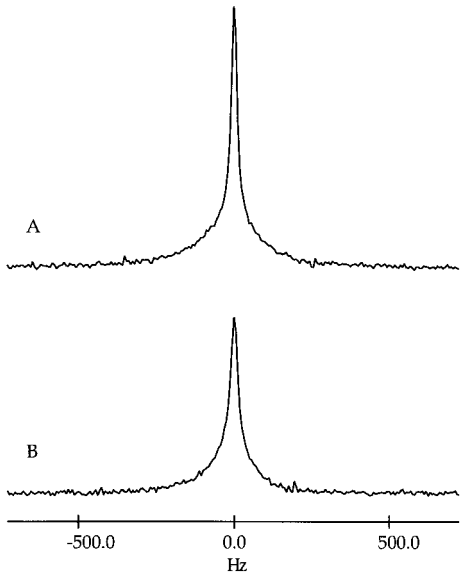

FIGURE 6: (A) ^{25}Mg NMR spectrum of 2 mM Mg^{2+} in 2 mg/mL actin solution in the presence of phalloidin. ATP in the buffer has been removed by dialysis. (B) ^{25}Mg spectrum in the presence of 0.1 mM ATP from the buffer for comparison (same as Figure 1B but plotted on a different frequency scale). The temperature is 30 °C.

then dialyzing the solution against ATP-free actin buffer. Control experiments show no sign of interaction between Mg^{2+} and phalloidin (data not shown). Figure 6A shows a ^{25}Mg NMR spectrum of 2 mM Mg^{2+} in a solution of 2 mg/mL phalloidin-stabilized F-actin filaments which is essentially free of ATP. For comparison, Figure 6B shows a spectrum when the regular ATP-containing buffer is used. Table 2 shows fitting parameters obtained from double Lorentzian fits of these spectra. It is clear that the broad component of the spectrum in Figure 6A is much narrower than in Figure 6B. Furthermore, the I_B:I_A ratio is higher for Figure 6B than 6A, because the broad component is more heavily weighted in Figure 6B. One obvious advantage of using phalloidin is that complications due to Mg^{2+} exchange with ATP are eliminated.

DISCUSSION

The ^{25}Mg NMR experiments reported here provide the first direct demonstration that F-actin binds Mg^{2+} in a loose, nonspecific manner that is expected for a polyelectrolyte. Based on the modest values that we have determined for the quadrupole constants, it appears that at least the majority of the F-actin-bound Mg^{2+} ions do not lose waters of hydration. The relatively short observed correlation times indicate significant rotational mobility of Mg^{2+} on the surface of the F-actin polymer. In contrast, if Mg^{2+} were binding to specific sites, then dehydration and significant rotational immobilization would be anticipated. The observed NMR behavior is quite similar to that found for the binding of Mg^{2+} and other multivalent cations to duplex DNA *(14, 23, 27*−*30)*.

Although the dynamics of Mg^{2+} in actin filament solution can be compared to that in DNA solutions, the two systems differ in some important respects. Unlike DNA, an actin filament at steady state constantly undergoes polymerization and depolymerization at the two distinct filament ends, in a process known as treadmilling *(31)*. Moreover, the critical

Table 2: Parameters Obtained by Fitting the ^{25}Mg NMR Spectra in Figure 6 to Double Lorentzian Line Shapes[a]

spectrum	I_A[b]	I_B[b]	I_B:I_A	W_A[b]	W_B[b]
Figure 6A	0.34	0.66	1.9	25.3	133.1
Figure 6B	0.30	0.70	2.3	20.6	206.5

[a] The linewidths of the two Lorentzian lines illustrate the broad component and the narrow component of the spectra. [b] I_A and I_B are the integrated intensities of the two fitted Lorentzian lines A and B with normalized total intensity, respectively, and W_A and W_B are the line widths of A and B in hertz, respectively.

concentration of a G-actin pool is quite sensitive to experimental conditions, especially changes of salt concentrations. In our experiments, the concentration of Mg^{2+} was kept constant at 2 mM, to ensure that actin polymerizes to near completion. However, if the Mg^{2+} concentration approaches 10 mM, bundling of actin filaments occurs. The actin concentration is also an important parameter because it strongly affects the solution hydrodynamics which in turn affect the mobility and perhaps the exchange rate of Mg^{2+}. Finally, the dynamics of Mg^{2+} in F-actin solution may depend on the filament length as well. To control such complications in a systematic manner, the following conditions are desirable. First, the solution should be free of ATP. Second, the lengths of the actin filaments should be well controlled by the severing proteins such as gelsolin. Third, the actin filaments should be stabilized so that the filament length does not vary with changes in solution conditions. Based on the results reported here, especially the experiment shown in Figure 6, it should be possible to satisfy all of these requirements.

The behavior of the ^{25}Mg signal during the bundling transition of actin filaments induced by $Co(NH_3)_6^{3+}$ is quite interesting. The monotonic decrease of the linewidths with increasing amount of the bundling agent indicates that the bound Mg^{2+} on the actin surface is being displaced by $Co(NH_3)_6^{3+}$. This observation again confirms our hypothesis that at least some of the Mg^{2+} ions on the actin filaments are bound nonspecifically and can be displaced by other cations. The loss of ^{25}Mg intensity during actin bundling, on the other hand, suggests that some of the Mg^{2+} ions are trapped as the titration with $Co(NH_3)_6^{3+}$ proceeds and the actin filaments form bundles. The bundling of the F-actin polyelectrolyte requires charge neutralization *(11)*, and the trapping of Mg^{2+} along with cobalt hexaammine cations may fulfill that requirement. When the bundling transition is reversed by K^+, the trapped Mg^{2+} ions are released. As a result, the observed ^{25}Mg intensity recovers and the linewidth broadens, as illustrated in Figure 4. In Figure 4, panel A is the spectrum of Mg^{2+} in bundled actin filament solution, and panel B shows the ^{25}Mg signal of the same sample after the actin bundles were partially dissolved by the addition of excess K^+. When actin bundling occurs, the broad components of the ^{25}Mg NMR signal are severely broadened. Since relaxation of the broadened components occurs during the spectrometer dead time, a large part of the broadened signal is not detected, which may explain the loss of ^{25}Mg intensity (Figure 3). Consequently, the detected signal is mainly composed of the narrow components. Even when some of the broad components of the signal are detected, they would appear to be very close to the baseline. An illustration of this is the simulated spectra in the Appendix: as the rotational correlation time increases, the signal first broadens, and then appears to sharpen as the broad components disappear into the baseline. In real experiments, some intensity from the broad components would likely be lost. Another contributing factor is that a part of the bound Mg^{2+} ions are released due to actin bundling and give narrow NMR signals. Overall, the ^{25}Mg spectrum appears to be narrower upon actin bundle formation. When the actin bundles are partially dissolved by K^+, Mg^{2+} ions are condensed on the filaments again, and part of the ^{25}Mg signal recovers with a 20% intensity increase when the broad components of the signal are detected. Consequently, the spectrum appears to be broadened again.

Different degrees of line broadening can have different effects on the apparent line shape. A case in point is a comparison between Figure 4 and Figure 6. In the case of Figure 6, ATP in the solution causes line broadening, and the line shape appears to be broader than in the absence of ATP. In Figure 4, however, the trapped Mg^{2+} ions experience severe broadening in the actin bundle solution that results in apparently sharp and single Lorentzian line shape. The main difference here is that severe line broadening is usually accompanied by intensity loss, as shown in Figure 3. Subsequently, Figure 4 displays the effect on line shape when severe broadening is reduced: the lost intensity is partially recovered, and the line shape appears to be broader.

The titration of Mg^{2+} in actin solution with ATP shows that anionic ATP can compete with actin filaments for binding to Mg^{2+} ions, consistent with the idea that Mg^{2+} ions bind to actin filament in a loose manner similar to counterion condensation on other polyelectrolytes such as DNA. Eventually the binding to ATP dominates at high concentrations of ATP, and the line shape changes from multi-Lorentzian to broad single-Lorentzian. While a moderately weak ($K_d = 10\ \mu M$) binding site for ATP on the surface of F-actin has been detected in various studies *(32)*, the effects of ATP on actin filament structure *(33, 34)* may relate partly or primarily to the selective depletion of condensed counterions from the surface of the actin filament.

It is worth mentioning that a technical concern must be addressed when comparing the signal intensities among the spectra obtained under different conditions. Because of the relatively strong binding of Mg^{2+} to actin filaments at the nonspecific sites, part of the broad component of the NMR signal relaxes fast enough to escape detection in solution NMR because of a long deadtime, which results in a certain intensity loss. Therefore, a direct comparison of intensities must be made with caution, and modest intensity losses might be anticipated even for nonspecific binding.

Our ^{25}Mg NMR data will help to clarify the interaction between Mg^{2+} and actin filaments under physiologically relevant conditions, for which the Mg^{2+} concentrations are typically in the millimolar range and the actin concentrations are in the mg/mL range. The polyelectrolyte behavior of actin filaments may prove crucial to their biological function. The data presented here demonstrate that the interaction of F-actin with Mg^{2+} reflects this polyelectrolyte behavior. We have yet to address issues such as the exchange dynamics of Mg^{2+} in actin filament solutions. It should also be noted that our solution NMR experiments omit the physiological packing constraints inside cells due to the presence of other proteins that can be potentially important *(35)*.

Metal ions play indispensable structural and functional roles in virtually every biological tissue. Mg^{2+}, for example, is an essential factor in the activity of more than 300 enzymes. There have been extensive studies on metal ions as specific protein-binding ligands, which play important roles in signal transduction, electron transfer, etc. However, the mechanisms of its interaction with many cytoskeletal elements including F-actin, microtubules, and intermediate filaments have yet to be understood at a fundamental level. Therefore, further NMR studies on the interactions between Mg^{2+} and not only actin filaments but also potentially other biological filaments such as microtubules and intermediate filaments are biophysically and physiologically important.

APPENDIX

Line Shape Simulation of ^{25}Mg NMR. The NMR line shapes of $I = {}^5/_2$ and $I = {}^7/_2$ nuclei and the effect of chemical exchange on line shape are described in detail by Westlund and Wennerström (*20*). Here we briefly outline line shape analysis for $^{25}Mg^{2+}$, a spin $I = {}^5/_2$ nucleus, as described in Westlund and Wennerström's paper.

The time derivative of the magnetization vector of $I + {}^1/_2$ elements is

$$\frac{d\underline{\chi}}{dt} = -(i\omega_0\mathbf{E} + \mathbf{P})\underline{\chi} \qquad (1)$$

Here **E** is a unit matrix and **P** is a transverse relaxation matrix in the following form:

$$\mathbf{p} = \begin{pmatrix} A & E & 0 \\ E & \mathrm{B} & \mathrm{F} \\ 0 & F & C \end{pmatrix} K,\ K = \frac{1}{125}\left(\frac{eQ}{\hbar}\right)^2$$

where

$$A = 3J_0 + 5J_1 + 2J_2 + iQ_1 + 2iQ_2$$

$$B = \frac{1}{24}(123J_0 + 370J_1 + 497J_2 + 126iQ_1 - 3iQ_2)$$

$$C = \frac{5}{12}(3J_0 + 26J_1 + 16J_2 - 6iQ_1 + 9iQ_2)$$

$$E = \frac{27}{2\sqrt{21}}(J_0 - J_2 + 2iQ_1 - iQ_2)$$

$$F = -\frac{25}{12\sqrt{14}}(3J_0 + 14J_1 - 17J_2 + 6iQ_1 - 3iQ_2)$$

J and Q are spectral densities which are expressed as

$$J(n) = \frac{\tau_c}{1 + (n\omega\tau_c)^2}$$

$$Q(n) = \frac{n\omega\tau_c{}^2}{1 + (n\omega\tau_c)^2}$$

A Fourier transform of eq 1 yields a set of three linear equations:

$$\underline{x}(0) = \{i(\omega_0 - \omega)\mathbf{E} + \mathbf{P}\}\underline{\tilde{x}}(\omega)$$

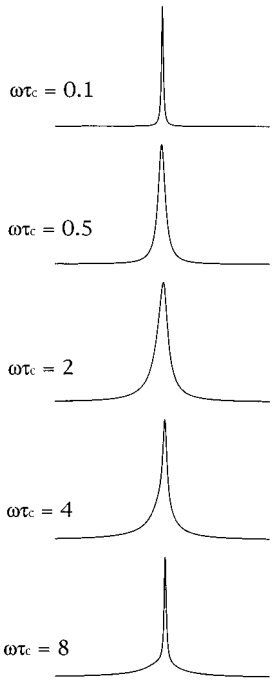

FIGURE 7: Simulated spectra as $\omega\tau_c$ changes. All spectra have the same arbitrary spectral widths that are scaled by the quadrupole coupling constant χ (not specified). Chemical exchange effect is not included. All spectra are scaled to the same height.

The line shape $I(\omega)$, a sum of three different Lorentzians, can be derived as

$$I(\omega) = \mathrm{Re}\{\mathbf{X}^*[i(\omega_0 - \omega)\mathbf{E} + \mathbf{P}]^{-1}\mathbf{X}\}$$

The line shape $I(\omega)$ can be simulated by assuming the rotational correlation time τ_0. Chemical exchange will affect the line shape. For a two-site exchange, elements A, B, and C of the relaxation matrix **P** are modified to include the exchange effect, as described in detail by Westlund and Wennerstrom (*20*).

Figure 7 shows simulated line shapes at different $\omega\tau_0$ values. The progression of the line shape as a function of $\omega\tau_c$ shows a sequence of interesting changes: the line width (half-height width) first broadens, but the overall line shape maintains Lorentzian; as broadening continues, the overall line shape appears to be distinctly non-Lorentzian, and the line width becomes narrow again. The asymmetric line shapes are due to dynamic shifts.

ACKNOWLEDGMENT

Dr. Hong Deng is gratefully acknowledged for helpful discussions and for developing the programs used in this work.

REFERENCES

1. Anderson, C. F., and Record, M. T., Jr. (1990) *Annu. Rev. Biophys. Biophys. Chem. 19*, 423−465.
2. Harned, H. S., and Owen, B. B. (1958) *The physical chemistry of electrolyte solutions*, Reinhold, New York.
3. Manning, G. S. (1969) *J. Chem. Phys. 51*, 924−933.
4. Manning, G. S. (1972) *Annu. Rev. Phys. Chem. 23*, 117−140.
5. Manning, G. S. (1978) *Q. Rev. Biophys. 11*, 179−246.
6. Manning, G. S. (1996) *Ber. Bunsen-Ges. Phys. Chem. 100*, 909−922.

7. Fuoss, R. M., Katchalsky, A., and Lifson, S. (1951) *Proc. Natl. Acad. Sci. U.S.A. 37*, 579−589.
8. Le Bret, M., and Zimm, B. H. (1984) *Biopolymers 23*, 287−312.
9. Schmitz, K. S. (1993) *Macroions in Solution and Colloidal Suspension*, VCH, New York.
10. Young, M. A., Jayaram, B., and Beveridge, D. L. (1997) *J. Am. Chem. Soc. 119*, 59−69.
11. Tang, J. X., and Janmey, P. A. (1996) *J. Biol. Chem. 271*, 8556−8563.
12. Tang, J. X., Wong, S., Tran, P. T., and Janmey, P. A. (1996) *Ber. Bunsen-Ges. Phys. Chem. 100*, 796−806.
13. Bloomfield, V. A. (1991) *Biopolymers 31*, 1471−1481.
14. Braunlin, W. H. (1995) *Adv. Biophys. Chem. 5*, 89−139.
15. Strzelecka, G. H., Prochniewicz, E., and Drabikowski, W. (1978) *Eur. J. Biochem. 88*, 229−237.
16. Bryant, R. G. (1972) *J. Magn. Reson. 6*, 159−166.
17. Forsén, S., and Lindman B. (1981) *Methods Biochem. Anal. 27*, 289−486.
18. Spudich, J., and Watt, S. (1971) *J. Biol. Chem. 246*, 4866−4871.
19. Suzuki, A., Maeda, T., and Ito, T. (1991). *Biophys. J. 59*, 25−30.
20. Westlund, P.-O., and Wennerström, H. (1982) *J. Magn. Reson. 50*, 451−466.
21. Deng, H. (1995) Ph.D. Dissertation, The University of Nebraska-Lincoln.
22. Bock, J. L., Crull, G. B., Wishnia, A., and Springer, C. S. J. (1991) *J. Inorg. Biochem. 44*, 79−87.
23. Berggren, E., Nordenskiöld, L., and Braunlin, W. H. (1992) *Biopolymers 32*, 1339−1350.
24. Doi, M., and Edwards, S. F. (1986) *The Theory of Polymer Dynamics*, Clarendon Press, Oxford.
25. Eimer, W., and Pecora, R. (1991) *J. Chem. Phys. 94*, 2324−2329.
26. Prochniewicz, E., Zhang, Q., Janmey, P., and Thomas, D. (1996) *J. Mol. Biol. 260*, 756−766.
27. Reimarsson, P., Parello, J., Drakenberg, T., Gustavsson, H., and Lindman, B. (1979) *FEBS Lett. 108*, 439−442.
28. Rose, D. M., Bleam, M. L., Record, M. T., Jr., and Bryant, R. G. (1980) *Proc. Natl. Acad. Sci. U.S.A. 77*, 6289−6292.
29. Rose, D. M., Polnaszek, C. F., and Bryant, R. G. (1982) *Biopolymers 21*, 653−664.
30. Braunlin, W. H., Nordenskiold, L., and Drakenberg, T. (1991) *Biopolymers 31*, 1343−1346.
31. Wegner, A. (1982) *J. Mol. Biol. 161*, 607−615.
32. Kiessling, P., Polzar, B., and Mannherz, H. (1993) *Biol. Chem. Hoppe-Seyler 374*, 183−192.
33. Janmey, P. A., Hvidt, S., Oster, G. F., Lamb, J., Stossel, T. P., and Hartwig, J. H. (1990) *Nature 347*, 95−99.
34. Suzuki, S., Noda, H., and Maruyama, K. (1973) *J. Biochem. (Tokyo) 73*(4), 695−703.
35. Tang, J. X., Ito, T., Tao, T., Traub, P., and Janmey, P. A. (1997) *Biochemistry 36*, 12600−12607.
36. Wright, L. A., and Lerner, L. E. (1994) *Biopolymers 34*, 691−700.

BI982301F